Procedia Computer Science

Volume 51, 2015, Pages 2533–2542

ICCS 2015 International Conference On Computational Science

A DDDAS Plume Monitoring System with Reduced Kalman Filter *

Liqian Peng[1,3], Matthew Silic[1,3], and Kamran Mohseni[1,2,3]

[1] Department of Mechanical and Aerospace Engineering,
[2] Department of Electrical and Computer Engineering,
[3] Institute for Networked Autonomous Systems,
University of Florida, Gainesville, FL, 32611
{liqianpeng, msilic, mohseni}@ufl.edu

Abstract

A new dynamic data-driven application system (DDDAS) is proposed in this article to dynamically estimate a concentration plume and to plan optimal paths for unmanned aerial vehicles (UAVs) equipped with environmental sensors. The proposed DDDAS dynamically incorporates measured data from UAVs into an environmental simulation while simultaneously steering measurement processes. The main idea is to employ a few time-evolving proper orthogonal decomposition (POD) modes to simulate a coupled linear system, and to simultaneously measure plume concentration and plume source distribution via a reduced Kalman filter. In order to maximize the information gain, UAVs are dynamically driven to hot spots chosen based on the POD modes using a greedy algorithm. We demonstrate the efficacy of the data assimilation and control strategies in a numerical simulation and a field test.

Keywords: DDDAS, plume monitoring, reduced Kalman filter, UAV, POD

1 Introduction

The use of cooperative, small unmanned aerial vehicles (UAVs) equipped with simple environmental sensors provides a promising option for safe and cost-effective data collection. Two benefits of such a system are the relatively low-cost of individual vehicles and the safety of using unmanned vehicles for missions involving harsh atmospheric conditions or toxic environments. Regardless of the number of UAVs employed in an application, the key consideration in the use of UAVs is how to position them in order to gain useful information from their locations and/or path. Dynamic data driven application systems (DDDAS) provide a means to position the UAVs in an efficient manner using the real time data obtained from the sensors. The framework of DDDAS is driven by the goal of dynamically incorporating data into

*The authors gratefully acknowledge the support of the Air Force Office of Scientific Research (AFOSR).

doi:10.1016/j.procs.2015.05.361

a running application (e.g. an environmental simulation) while simultaneously using the application to steer measurement processes [2]. The DDDAS framework is widely used in wildfire simulation [11, 18], identification of airborne contaminants [1, 9], and weather forecasting [4].

This article is an extension of our previous work in plume monitoring using UAVs [12, 13]. A new data assimilation technique based on a reduced Kalman filter (RKF) is proposed for two-dimensional plume evolution problem. The plume is released upwind of two square obstacles (representing buildings) and travels downstream according to the advection-diffusion equation. For real-time plume simulation and estimation, the unknown parameters in our problem include not only the initial condition of the plume concentration, but also the plume source distribution. This leads to an inverse problem with high-dimensional control spaces in the form of unknown parameters, and whose solution is not unique. This motivates the construction of reduced-order surrogate models to uniquely determine these parameters in DDDAS. The proper orthogonal decomposition (POD) [5] can be used to replace a high-dimensional Kalman filter with a RKF while preserving the dominant features of the original filter. The RKF is applied to incorporate point observations into a coupled dynamic systems to simultaneously estimate plume concentration and plume source distribution. Compared with the least square method that was applied in [12] for plume estimation, the RKF can obtain more robust and accurate results, because all the historical data is accumulated for current plume estimation.

The remainder of this article is organized as follows. In Section 2, we first formulate the problem of plume evolution within an urban environment; then discuss and present the DDDAS methodology, focusing on the RKF for the data assimilation procedure. Section 3 and Section 4 provide a numerical simulation and a field test, respectively. Finally, conclusions are offered in Section 5.

2 DDDAS methodology

The DDDAS is a systems-level approach and can be applied to many phenomena where good simulation models are available. Here, we focus on measuring and tracking a concentration plume from sparse observations in an advection-diffusion system described by

$$\frac{\partial \psi}{\partial t} + v \cdot \nabla \psi = \frac{1}{Pe} \nabla^2 \psi + f + \xi; \qquad \psi(0, x) = \psi_0(x), \tag{1}$$

where $t \in [0, T]$ denotes the time, $x \in \Omega$ is the space coordinate, $v = v(t, x)$ is the background wind velocity, Pe is the Péclet number which quantifies the relative strength of the advection and diffusion terms, $\psi(t, x)$ is the concentration field, $f(t, x)$ is the plume source distribution, $\xi(t, x)$ is the small noise introduced by the uncertainty in the background velocity field, the diffusion constant, or the concentration source, and $\|\xi\| \ll \|f\|$. We examine the case where a plume source distribution is described by a linear stochastic equation, which is advected under the action of the velocity field v while also dispersing due to the diffusion. Suppose the domain Ω is discretized into n grid points , and the discrete version of the advection diffusion equation at time step k is given by $\psi_k = A_{k-1}\psi_{k-1} + f_{k-1}\delta t + \xi_{k-1}$, and the plume source distribution is evolved by $f_k = A'_{k-1} f_{k-1} + \eta_{k-1}$, where $\psi_k, f_k, \xi_k, \eta_k \in \mathbb{R}^n$, δt denotes the unit step, η_k denotes the uncertainty of the evolution of plume source distribution. If we assume the plume source distribution f_k is governed only by the stochastic noise, then $A'_k = I$. The coupled system for plume concentration and plume source distribution is given by

$$\begin{bmatrix} \psi_k \\ f_k \end{bmatrix} = \begin{bmatrix} A_{k-1} & \delta t \cdot I \\ 0 & A'_{k-1} \end{bmatrix} \begin{bmatrix} \psi_{k-1} \\ f_{k-1} \end{bmatrix} + \begin{bmatrix} \xi_{k-1} \\ \eta_{k-1} \end{bmatrix}. \tag{2}$$

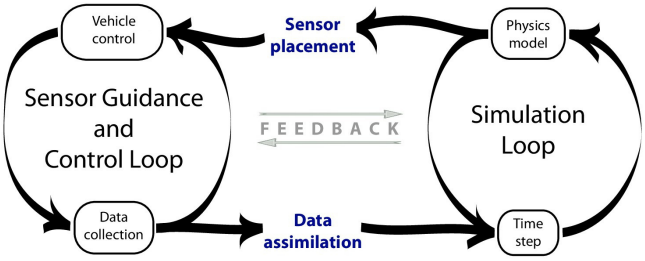

Figure 1: Schematic of the online DDDAS. The two main components of the system are a sensor guidance and control loop and a simulation loop. The two loops interact through data assimilation and sensor placement algorithms.

Suppose at each time step the plume concentration is measured at l ($l \ll n$) discrete points $s_1, s_2, ..., s_l$ with some sensor noise ζ, the observation of this system is given by

$$z_k = \begin{bmatrix} P_k^T & 0 \end{bmatrix} \begin{bmatrix} \psi_k \\ f_k \end{bmatrix} + \zeta_k, \tag{3}$$

where $P_k \in \mathbb{R}^{n \times l}$ and the ith column of P_k is the s_ith column of the identity matrix I_n. The wind velocity v can be obtained by a CFD model or weather forecasting. In this paper, v is found by numerically solving the incompressible Navier–Stoke equations using a finite difference method at n grid points. The wind velocity v and the linear operator A_k vary with time. Since mobile sensors can measure the plume concentration at different locations, P_k also varies with time. Therefore, (2) and (3) construct a linear time variant (LTV) system. For the case of a discrete plume of concentration being released, the forcing term f in (2) is zero for $t > 0$, and the coupled system degenerates to an ODE of $\psi \in \mathbb{R}^n$.

A schematic of this DDDAS system is shown in Figure 1. Since the number of measured grid points l at one time step is much smaller than the total number of grid points n in the whole space, the original discrete LTV system can be unobservable for a small time domain $[0, T]$ even if we ignore all the stochastic noise. To address this, an offline-online splitting methodology is applied to estimate the coupled variable (ψ, f) on a subspace $\mathcal{S}$ of $\mathbb{R}^{2n}$. In the offline stage, the wind velocity is obtained by solving the Navier–Stokes equations. Then we sample the possible plume source locations and solve the advection–diffusion equation, which results in possible trajectories of (ψ, f). In the final offline step, the dominant modes of (ψ, f) are identified by the POD method.

In the online stage, two coupled feedback loops are run in real-time to improve the accuracy of a running simulation while simultaneously improving the effectiveness of data collection strategies. We refer to the first loop in the DDDAS as the sensor guidance and control loop. The system components in this loop are responsible for movement, collision avoidance, and data collection. The second loop in the system is referred to as the simulation loop. In this loop, a real-time simulation attempts to model the physical system of interest; in our case, a concentration plume is modelled using the advection-diffusion equation mentioned above. The key to the DDDAS is an effective, two-way coupling between the simulation loop and the sensor guidance and control loop. This is accomplished by using a POD based data assimilation routine to assimilate data collected in the guidance and control loop into the running simulation loop, resulting in improved accuracy in the simulation. Meanwhile, in order to improve the data collection process, the simulation loop can be used to adaptively construct local POD

modes, which are then applied in the proposed sensor placement algorithm to steer the UAVs to impactful measurement locations.

In the rest of this section, we discuss each component of the the DDDAS plume monitoring system.

2.1 Sensor mobility control

Sensor mobility control refers to a strategy for gathering sensor measurements to support a sensing objective, such as environmental measurement. When the sensors are installed on robotic platforms an important part of the problem is planning the sensor path to achieve low working time or low energy consumption [7], obstacle avoidance in unstructured dynamic environments [8, 17, 14], or efficiently gather target information [20]. In this paper, we applied a hierarchical control strategy were proposed to maximize the useful information collected by mobile sensors. The detailed procedure can be found in [12]. Based on the speed limitation of UAVs, the entire time domain is artificially partitioned into N smaller subintervals such that during each subinterval, any UAV has the ability to reach (or at least approach) any important measurement location. At a higher level, a greedy algorithm was developed to find the the important positions, or hot spots, for a fixed time interval where sensors may obtain more information than arbitrarily chosen positions [12]. At a lower level, a Lyapunov vector field based scheme is used to guide UAVs to the chosen hot spots at each time interval [16].

2.2 Proper orthogonal decomposition

Since observations are incomplete and noisy, it is not sufficient to estimate the instant plume concentration and plume source distribution in the high dimensional space $\mathbb{R}^{2n}$ with the measured data alone. However, if we restrict this problem to a subspace $\mathcal{S}$ with a lower number of unknown parameters, the measured data is sufficient to find an approximate solution for plume concentration on $\mathcal{S}$ with high accuracy and low computational cost. The proper orthogonal decomposition method [10] is used to capture $\mathcal{S}$ in this article. The key idea of POD is to deliver a set of empirical eigenfunctions so that the original data is optimally captured by these modes in the least squares sense [5]. An empirical eigenfunction is often referred to as a POD mode. Hence although the original system (2) has a dimension of $2n$, the online simulation is computed by a reduced order equation with a significantly low dimension d. Specifically, Galerkin projection provides a lower dimensional approximation by projecting the full system onto a linear (or an affine) subspace.

2.3 Reduced Kalman filter (RKF)

For simplicity, we first consider a determinant system and ignore all the stochastic noise in (2) and (3). Suppose the approximation of ψ_k and f_k is given by $[\hat{\psi}_k; \hat{f}_k] = \Phi c_k$, the reduced system based on the Galerkin projection is given by

$$c_k = \tilde{A}_{k-1} c_{k-1}, \tag{4}$$

where $\tilde{A}_{k-1}$ denotes the projected linear operator of $[A_{k-1}\ \delta t \cdot I; 0\ A'_{k-1}]$. The observation is given by

$$z_k = \tilde{P}_k^T \Phi c_k \tag{5}$$

where $\tilde{P}_k^T = [P_k^T\ 0] \in \mathbb{R}^{2n \times d}$, and $\Phi = [[\varphi_1; \phi_1], ..., [\varphi_d; \phi_d]] \in \mathbb{R}^{2n \times d}$ denotes the POD basis for the coupled variable (ψ, f). A RKF can be used to assimilate measured data into the

running simulation (and couple the simulation loop to the control loop). It has been applied in data assimilation in the oceanic and atmospheric research [3, 6]. The state of the filter is represented by a state estimate at time k and the error covariance matrix (a measure of the estimated accuracy of the state estimate). In this paper, the RKF is constructed by the Galerkin projection for the Kalman equation, which is conceptualized as a prediction stage and a correlation stage. The prediction stage uses (4) to produce an updated estimate of the state at the current time step. This priori state estimate $c_k^- \in \mathbb{R}^d$ does not include observation information from the current time step. A priori estimate error covariance $P_k^- \in \mathbb{R}^{d\times d}$ is updated as

$$P_k^- = \tilde{A}_{k-1} P_{k-1} \tilde{A}_{k-1}^T + \tilde{Q}, \tag{6}$$

where $\tilde{Q} = \Phi^T Q \Phi = c_1 I \in \mathbb{R}^{d\times d}$ is the reduced order covariance matrix for $\tilde{\omega}_k$.

In the update phase, the current a priori prediction is combined with current observation at selected positions to refine the state estimate. In particular, the Kalman gain, $K_k \in \mathbb{R}^{d\times m}$, can be computed as

$$K_k = P_k^- \tilde{H}_k^T (\tilde{H}_k P_k^- \tilde{H}_k^T + R)^{-1}. \tag{7}$$

where $\tilde{H}_k = H_k \Phi \in \mathbb{R}^{m\times d}$. A posteriori state estimate is generated by the following equation,

$$\tilde{\psi}_k = \tilde{\psi}_k^- + K_k(z_k - \tilde{H}_k \tilde{\psi}_k^-), \tag{8}$$

and the covariance matrix is updated as

$$P_k = P_k^- - K_k \tilde{H}_k P_k^-. \tag{9}$$

Equations (4)–(9) have a similar form as the standard Kalman filter. However, since the state variable and covariance matrix are updated in a low dimensional subspace, significant speedups can be obtained by the RKF.

3 Simulation

The proposed data assimilation and control strategy described above are shown to successfully monitor and characterize a simulated concentration plume that is analogous to the release of an airborne plume of toxic chemicals in an urban environment. The plume motion is governed by the advection-diffusion equation given in (1). For simplicity, the initial plume concentration is zero. The plume source distribution is a constant. However, in this test, neither the precise location nor the extent of the plume source distribution is known. As time progresses the DDDAS is able to identify and update the plume concentration and plume source distribution by guiding the UAVs to measure plume concentration near hot spots while assimilating the data measured along the sensor paths. All variables, including time, length, and velocity, are given in nondimensional units unless otherwise specified.

In the simulation, the wind velocity is computed by solving the non-dimensional Navier–Stoke equation on the spatial domain $\Omega = [0, 30] \times [0, 10]$ (see Figure 2), which is treated as the "real wind". Two square obstacles are placed within the domain to simulate buildings in an urban environment. All concentration plume boundary conditions are set to $\psi = 0$ for simplicity. As the concentration field evolves, the plume interacts with the buildings in the domain, passing between and around them. For time $t > 0$, a plume source distribution is set as $f(t, x) = 1.2\exp(-||x - x_1||_2^2) + 0.8\exp(-||x - x_2||_2^2)$ with stochastic evolution where $x_1 = (2.3, 4.1)$ and $x_2 = (2.7, 5.5)$ (See Figure 3). This will be used as the true plume solution and as a reference for all measures of accuracy. The total time domain of interest is $[0, 30]$ from

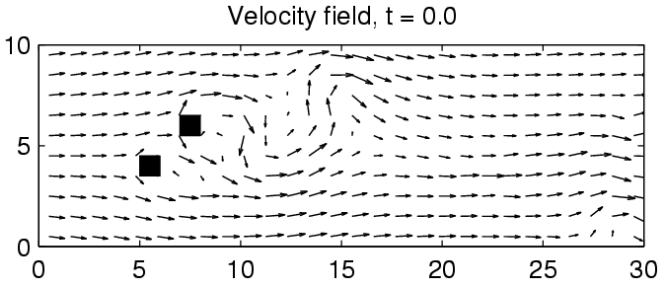

Figure 2: The background wind velocity field at $t = 0$. The dimensionless unit is used for both spatial and temporal coordinates.

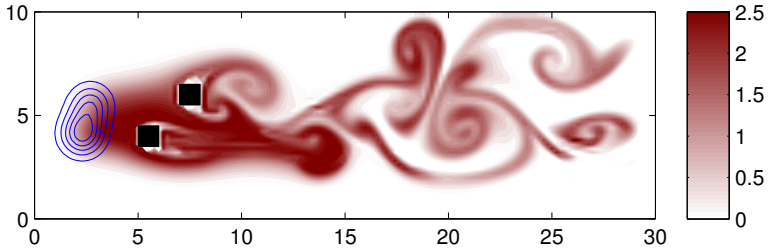

Figure 3: The red background shows the instantaneousness plume concentration $\psi(t, x)$ of the "real plume" for $t = 30$. The blue lines show the contour of the plume source $f(t, x) = 1.2\exp(-||x - x_1||_2^2) + 0.8\exp(-||x - x_2||_2^2)$.

the release of plume source to the time for the front of the plume to reach the right edge of the spatial domain.

The DDDAS described in previous sections is then applied to this data set. In the offline stage, the plume source distribution is assumed to be unknown so it is initially estimated to be within the square region $[1.5, 3.5] \times [3.5, 6.5]$. A linear combination of kernel functions is used to approximate the real plume source distribution. The kernel functions used here are set as $\hat{f}_i(x) = 0.1\exp(-||x - x_i||_2^2/0.8^2)$. The centers x_i of these Gaussian kernel functions are located on the grid points at 2, 2.5, 3 in horizontal direction and 4, 4.5, 5, 5.5, 6 in vertical direction. Using these kernel functions for plume source distribution, we generate corresponding trajectories for the evolution of plume concentration and build a discrete data ensemble. The POD method is then used to capture the dominant modes for the data ensemble. The contribution of each mode to the data ensemble is characterized by the corresponding singular value. If fixed sensors are used to measure the plume concentration, we take all the snapshots from the data ensemble. However, if UAVs are used, we can artificially partition the global time domain into 6 periods, and focus on the local POD modes for each time interval. Compared with global POD, local POD can fit the empirical data with higher accuracy for the same number of modes. In order to balance accuracy and computational speed, only the first three local POD modes are used to approximate the real plume concentration.

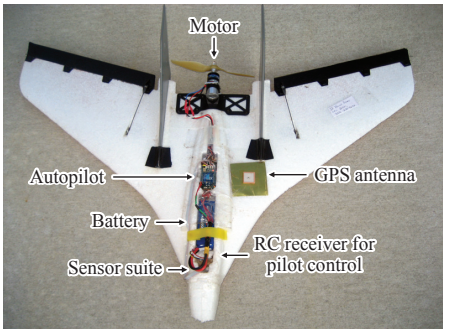

Figure 4: The resource constrained delta-wing UAV used in the experimental demonstration of the DDDAS technique. The 0.8 m wingspan UAV is equipped with a GPS sensor for position, a roll rate sensor, XBee wireless communication radio, and an autopilot to control the craft during autonomous mode.

4 Experiment

In order to verify the feasibility of this DDDAS in a real world application, we combine the aforementioned simulation with a field test involving three small, resource constrained UAVs. The experiment was designed to compare the performance of the DDDAS technique using real mobile sensors to the performance using simulated mobile sensors. The UAV GPS coordinates are continuously communicated to a ground station laptop, running the data assimilation and sensor placement loops in real time. The same virtual plume used in simulations is "measured" using the GPS coordinates of UAVs at a specified time. The UAVs are guided through the environment using Lyapunov guidance vector fields [16].

4.1 Hardware description

The small, resource constrained UAV used in the experiment is shown in Figure 4. The aircraft has a wingspan of 0.8 m and weighs less than 0.5 kg. The airframe, elevons, flaps, nose cone, propeller and servos, are all mass produced thus making the aircraft inexpensive compared to a custom design. This aircraft has been successfully used in several experiments in our research group and has proven itself robust, relatively simple and inexpensive to maintain, and easily replaceable if needed [19]. Additionally, the small size and simplicity of the aircraft allow for rapid deployment in areas that are not ideal for traditional UAVs. The Delta-Wing UAVs are equipped with a custom autopilot to allow for implementation of custom control strategies [16]. Several studies [19, 15] have shown that it is possible to achieve fully autonomous operation of a small UAV by means of this simple autopilot equipped with a limited number of sensors.

The autopilot consists of an on-board processor, a single axis rate gyro to sense roll rates, an absolute pressure sensor for altitude sensing, and a GPS receiver for positioning. The program has built-in routines to account for short term blackouts in the GPS signals and the noise and drifts in the sensors. The autopilot system also includes a complementary ground station that receives and relays data to and from the autopilot on board the aircraft. The autopilot transmits telemetry data to the ground station which responds with an updated position of the hot spot. As required by FAA regulations, the pilot remains in control at all times and can disengage the autopilot immediately if needed.

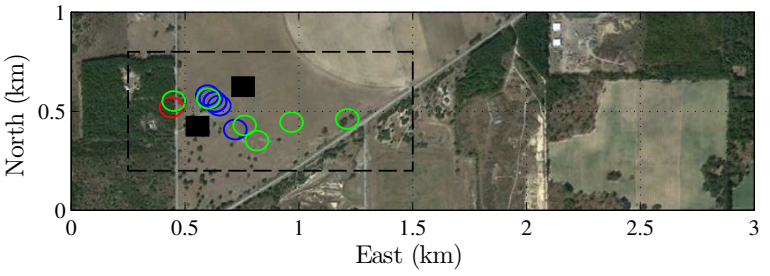

Figure 5: The experiment domain and hot spots.

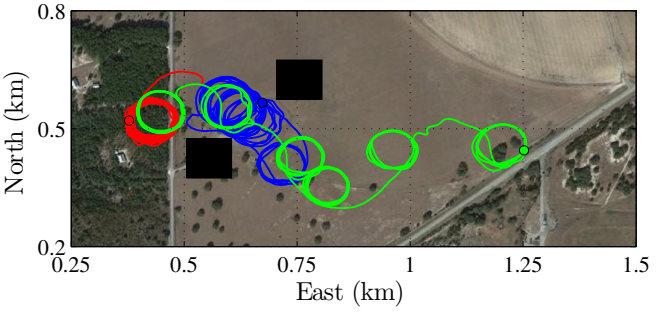

Figure 6: The GPS coordinates of three UAVs during approximately 12 minute of the field test.

4.2 Experiment results

The simulated plume concentration was applied on a 3×1 km domain with a time scale of 12 minute. Figure 5 plots the region that we take the experiment with accompanying "buildings". The circles correspond to three hot spots of the first three local POD modes. The hot spots are calculated based on the greedy algorithm discuss in [12]. Based on our simulation setup, the first hot spot (red) stays near the plume source, the second one (blue) is around the building area, and the third one (green) moves toward the right region as plume is advected by wind. The radius of each hot spot (50 m) corresponds to the turning radius of the delta-wing UAVs. The dashed box represents the boundary as shown in Figure 6. The red, green, and blue lines indicate the path of the three UAVs during this period of time.

Figure 7 shows the the percent error versus time in the estimated concentration plume. The error was computed using the ℓ^2 norm using fixed sensors and mobile sensors (both in experiment and simulation). Once UAVs achieve the desired locations, this DDDAS technique using three mobile sensors is able to reduce the error between the estimated concentration and the actual concentration to levels within approximately 20%. Despite the experimental uncertainties, this DDDAS technique using three real mobile sensors (subject to experimental uncertainty) matches very well with the simulated sensors. Most importantly, the results show that three mobile sensors are able to decrease the error between the estimated and actual concentration fields faster and to lower levels than ten static sensors.

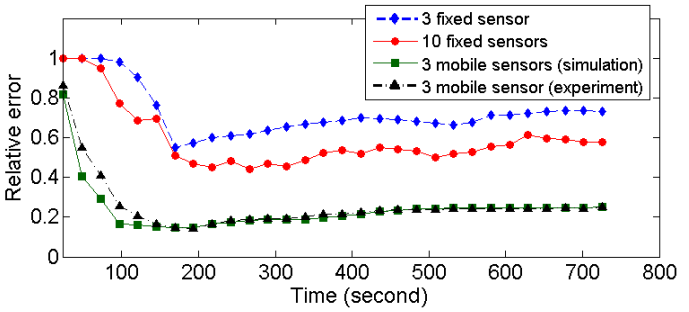

Figure 7: Percent error versus time for the DDDAS experiment.

5 Conclusions

In this article, we propose a complete dynamic data-driven application system (DDDAS) for simultaneously measuring and simulating a concentration plume and the plume source distribution in a dynamic environment. The dynamic evolution of plume concentration is governed by a coupled ODE. In order to assimilate incomplete and noisy state observations into this system in real-time, an offline-online approach is used. In the offline stage, we build a database by sampling several possible plume source regions and solving the governing equation to obtain possible trajectories for the plume concentration. We then use the proper orthogonal decomposition (POD) to find a few dominant modes. In the online stage, the reduced Kalman filter (RKF) is applied to estimate plume concentration and plume source distribution, which restricted to the subspace of the POD modes. The RFP-based data assimilation method leads to a hierarchical vehicle control strategy. On one level, hot spots are chosen such that maximal information can be obtained by UAVs. On another level, the Lyapunov vector field based scheme is used for vehicle path planning and control. Both the assimilation method and the control strategies are very computationally efficient and can be carried out in real time.

The proposed DDDAS combines the data assimilation method and control strategy together for plume characterization and the simulation/experiment results verify the utility of the system. Specifically, a small number of mobile sensors are able to approach the hot spots and produce a greatly improved estimate of plume concentration when compared to the use of many more static sensors. Moreover, experimental results using UAVs match very well with simulation results for plume estimation.

Acknowledgments

The authors wish to thank Richard O'Donnell for his help; his expertise in RC aircrafts and electronics facilitated the experiment.

References

[1] V. Akcelik, G. Biros, A. Drăgănescu, J. Hill, O. Ghattas, and B. van Bloeman Waanders. Dynamic data-driven inversion for terascale simulations: Real-time identification of airborne contaminants. In *Proceedings of the ACM/IEEE SC 2005 Conference*, pages 43–58, Seattle, WA, 2005.

[2] F. Darema. Dynamic data driven applications systems: A new paradigm for application simulations and measurements. *International Conference on Computational Science*, pages 662–669, 2004.

[3] B. F. Farrell and P. J. Ioannou. State estimation using a reduced-order Kalman filter. *Journal of the Atmospheric Sciences*, 58:3666–3680, 2001.

[4] M. Fisher, J. Nocedal, Y. Trémolet, and S. J. Wright. Data assimilation in weather forecasting: a case study in PDE-constrained optimization. *Optimization and Engineering*, 10:409 – 426, 2009.

[5] P.J. Holmes, J. L. Lumley, and G. Berkooz. *Turbulence, Coherent Structures, Dynamical Systems and Symmetry*. Cambridge Univ. Press, Cambridge, UK, 1998.

[6] I. Hoteit, D.-T. Pham, and J. Blum. A simplified reduced order Kalman filtering and application to altimetric data assimilation in Tropical Pacific. *Journal of Marine Systems*, 36:101–127, 2002.

[7] P.-M. Hsu, C.-L. Lin, and M.-Y. Yang. On the complete coverage path planning for mobile robots. *J. Intell. Robot. Syst.*, 74:945–963, 2014.

[8] A. Lazanas and J.-C. Latombe. Motion planning with uncertainty: A landmark approach. *Artif. Intell.*, 76:287–317, 1995.

[9] C. Lieberman, K. Fidkowski, K. Willcox, and B. van Bloemen Waanders. Hessian-based model reduction: Large-scale inversion and prediction. *Int. J. Numer. Meth. Fluids*, 71:135–150, 2013.

[10] M. Loève. *Probability Theory*. Van Nostrand, Princeton, N.J., 1955.

[11] J. Mandel, L. S. Bennethum, J. D. Beezley, J. L. Coen, C. C. Douglas, M. Kim, and A. Vodacek. A wildland fire model with data assimilation. *Mathematics and Computers in Simulation*, 79:584 – 606, 2008.

[12] L. Peng, D. Lipinski, and K. Mohseni. Dynamic data driven application system for plume estimation using UAVs. *J. Intell. Robot. Syst.*, 74:421–436, 2014.

[13] L. Peng and K. Mohseni. Sensor driven feedback for puff estimation using unmanned aerial vehicles. In *International Conference on Unmanned Aircraft Systems (ICUAS)*, pages 562 – 569, Orlando, FL, 2014.

[14] L. Peng, Y. Zhao, B. Tian, J. Zhang, B.-H. Wang, H.-T. Zhang, and T. Zhou. Consensus of self-driven agents with avoidance of collisions. *Phys. Rev. E*, 79(026113), 2009.

[15] W. J. Pisano, D. A. Lawrence, and K. Mohseni. Concentration gradient and information energy for decentralized UAV control. AIAA paper 2006-6459, AIAA Guidance, Navigation, and Control Conference and Exhibit, Keystone, CO, 2006.

[16] W. J. Pisano, D. A. Lawrence, and P. C. Peter. Autonomous UAV control using a 3-sensor autopilot. AIAA paper 2007-2756, AIAA Infotech Aerospace Conference, Rohnert Park, CA, 2007.

[17] N. S. V. Rao. Robot navigation in unknown generalized polygonal terrains using vision sensors. *IEEE Trans. Syst. Man Cybern*, 25:947–962, 1995.

[18] R. Rodríguez, A. Cortés, and T. Margalef. Injecting dynamic real-time data into a DDDAS for forest fire behavior prediction. In *Proceedings of the 9th International Conference on Computational Science*, volume 5545, pages 489 – 499, Baton Rouge, LA, 2009.

[19] A. Shaw and K. Mohseni. A fluid dynamic based coordination of a wireless sensor network of unmanned aerial vehicles: 3-D simulation and wireless communication characterization. *IEEE Sensors Journal*, 11:722–736, 2011.

[20] G. Zhang, S. Ferrari, and M. Qian. An information roadmap method for robotic sensor path planning. *J. Intell. Robot. Syst.*, 56:69–98, 2009.